

# On the effect of slip transfer at grain boundaries on the strength of FCC polycrystals

E. Nieto-Valeiras<sup>1,2</sup>, S. Haouala<sup>1</sup>, J. LLorca<sup>1,2,\*</sup>

<sup>1</sup>*IMDEA Materials Institute, C/ Eric Kandel 2, 28906 Getafe, Madrid, Spain*

<sup>2</sup>*Department of Materials Science, Polytechnic University of Madrid/Universidad Politécnica de Madrid, E. T. S. de Ingenieros de Caminos, 28040 Madrid, Spain*

---

## Abstract

The effect of slip transfer on the flow strength of various FCC polycrystals was analyzed by means of computational homogenization of a representative volume element of the microstructure. The crystal behavior was governed by a physically-based crystal plasticity model in the framework of finite strains where slip transfer at grain boundaries was allowed between slip systems suitably oriented according to geometrical criteria. Conversely, slip transfer was blocked if the conditions for slip transfer were not fulfilled, leading to the formation of dislocation pile-ups. All the model parameters for each material were identified from either dislocation dynamics simulations or experimental data from the literature. Slip transfer led to a reduction in the flow stress of the polycrystals (as compared with the simulations with opaque grain boundaries) which was dependent on the fraction of translucent and transparent grain boundaries in the microstructure. Moreover, dislocation densities and Von Mises stresses were much higher around opaque grain boundaries, which become suitable places for damage nucleation. Finally, predictions of the Hall-Petch effect in Al, Ni, Cu and Ag polycrystals including slip transfer were in better agreement with the literature results, as compared with predictions assuming that all grain boundaries are opaque, particularly for small grain sizes ( $< 20 \mu\text{m}$ ).

*Keywords:* Hall-Petch effect, crystal plasticity, polycrystal

---

\*Corresponding author; Email address: javier.llorca@imdea.org

## 1. Introduction

Metallic materials stand for ideal candidates for a wide range of structural applications in automotive, aerospace, chemical, construction and biomedical sectors owing to their high stiffness, formability and ductility. However, the strength of pure metals is very low for many applications due to the development of plastic deformation by dislocation slip. Hence, they have to be strengthened by obstacles that hinder dislocation motion and grain boundaries (GBs) stand among the strongest barriers to dislocation slip in polycrystals. Following Bayerschen et al. (2016), the interactions of dislocations with GBs can be grouped in three categories. Opaque or impenetrable GBs do not allow the propagation of dislocation slip through the boundary, leading to the formation of dislocation pile-ups and local stress concentrations (Friedman and Chrzan, 1998; Bieler et al., 2014). Moreover, the accumulation of dislocations at the GB induces strong strain gradients in order to preserve the displacement continuity between neighbor grains (Hughes et al., 2003). Conversely, transparent GBs are found when all the active slip systems are suitably aligned and the dislocations gliding in the incoming grain can be transmitted to the neighbor grain with no induced stress concentration. Finally, dislocations in some active slip systems can easily propagate through the boundary while others are blocked in the case of translucent GBs. This phenomenon leads to stress concentrations at the GB that depend on the number and intensity of slip in the systems blocked at the GB.

The effect of GBs on the strength of polycrystals was recognized in the 1950's, leading to the phenomenological Hall-Petch law (Hall, 1951; Petch, 1953) that relates the yield strength of the polycrystal,  $\sigma_y$  with the average grain size,  $\bar{D}_g$ , according to

$$\sigma_y = \sigma_\infty + C_{HP} \bar{D}_g^{-x} \quad (1)$$

where  $\sigma_\infty$  is the yield stress of a polycrystal with a very large grain size,  $C_{HP}$  a material constant and  $x$  a scaling exponent in the range -0.5 to -1 for many metallic alloys (Raj and Pharr, 1986; Dunstan and Bushby, 2013, 2014; Li et al., 2016). This expression is supported by different theoretical

models. For instance, Ashby (1970) proposed a physically-based model based on the strain incompatibility between grains with different orientations within a polycrystal. In this model, the total density of dislocations arises from two distinct contributions termed statistically stored dislocations (SSDs) and geometrically necessary dislocations (GNDs). The contribution of GNDs depends on the grain size and concentrates at the GBs whereas the density of SSDs is size independent. Other theoretical approaches also provided a rational explanation of the Hall-Petch law with a grain representation formed by a soft core surrounded by hard shell around the grain boundary (Kocks, 1970; Hirth, 1972).

Understanding the mechanical behavior of polycrystals has progressed rapidly in recent years through the combination of computational homogenization and crystal plasticity constitutive models (Segurado et al., 2018). Within this framework, two different strategies have been used to study the effect of GBs on the strength of polycrystals based on either strain-gradient or physically-based crystal plasticity models. In the former, a length scale is introduced in the crystal plasticity constitutive equation through the plastic strain gradients, which are related to the density of GNDs near the grain boundaries through the Nye tensor (Nye, 1953). Different investigations have used this approach to analyze the effect of grain size on the strength of polycrystals (Acharya and Beaudoin, 2000; Cheong et al., 2005; Bayley et al., 2007; Bargmann et al., 2010; Lebensohn and Needleman, 2016). Nevertheless, the comparisons with the abundant available experimental data were not fully convincing because most of the simulations were limited to small representative volume elements (RVEs) of the microstructure having only a few dozens of grains due to computational limitations. They were overcome by Haouala et al. (2020b), who determined the effect of grain size on the strength of different FCC polycrystals by means of computational homogenization of RVEs containing several hundred grains using a Fast Fourier Transform in combination with a strain gradient crystal plasticity model. The density of GNDs resulting from the incompatibility of plastic deformation among different crystals was obtained from the Nye tensor, which was efficiently obtained from the curl operation in the Fourier space. The simulation results were in good agreement with the experimental data for Cu, Al, Ag and Ni polycrystals for grain sizes  $> 20 \mu\text{m}$ . Similar results were also obtained by Rubio et al. (2019) through computational homogenization of equivalent RVEs using the finite element method and a physically-based crystal plasticity model

that takes into account the storage of dislocations near the grain boundaries, following the approach developed by Haouala et al. (2018). Interestingly, the predictions of the physically-based model also overestimated the strength of the polycrystals when the average grain size was  $< 20 \mu\text{m}$ . It was argued that the differences between experimental data and simulation results (using either strain gradient or physically-based models) arose because all GBs were assumed to be opaque in the simulations.

There is ample experimental evidence indicating that slip transfer through the GBs can take place (Shen et al., 1988; Lee et al., 1989) and is often associated with a good alignment between incoming and outgoing slip systems. Thus, geometrical criteria based on the orientation of the grains and slip systems across the boundary have been used to analyze slip transfer. The geometrical parameters used to predict slip transfer between two slip systems on either side of a GB are defined in Fig. 1. They are the angle  $\kappa$  between the Burgers vectors of the dislocations in the incoming ( $\mathbf{b}_\alpha$ ) and outgoing ( $\mathbf{b}_\beta$ ) slip plane, the angle  $\psi$  between the slip plane normals ( $\mathbf{n}_\alpha$  and  $\mathbf{n}_\beta$ ) and the angle  $\theta$  between the two slip plane intersections with the GB plane.

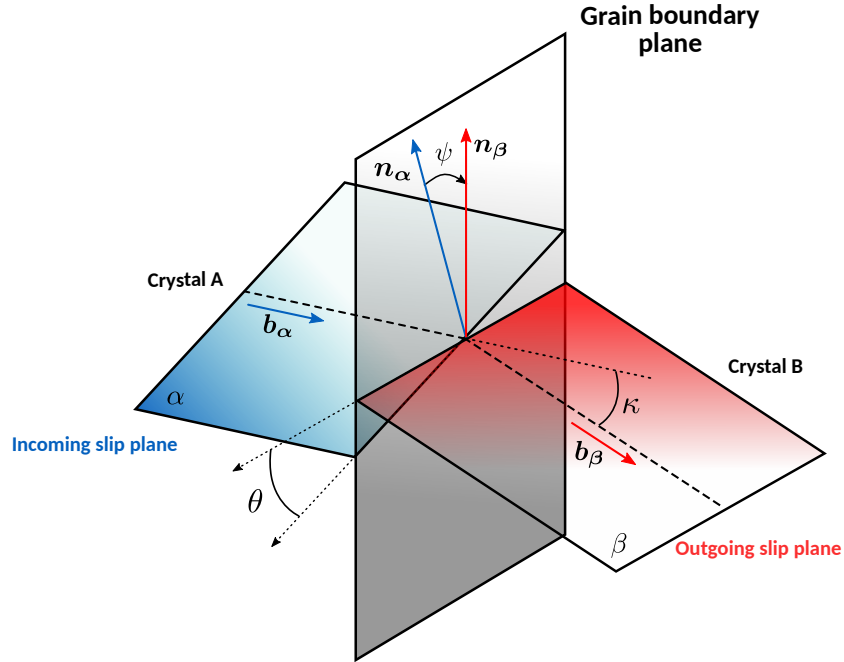


Figure 1: Geometrical parameters to assess slip transfer across the GB.

The experimental evidence indicates that slip transfer takes place more easily in low-angle GBs, i.e. when the misorientation angle between adjacent grains is below  $\approx 15^\circ$  (Read and Shockley, 1950). Nevertheless, slip transfer is not guaranteed at low-angle GBs, not it is impossible at large GB misorientations. Based on *in situ* TEM deformation experiments, Lee et al. (1989) proposed another slip transfer criterion from grain A to grain B. The so-called *LRB* parameter was expressed by

$$LRB = \cos \theta \cos \kappa \quad (2)$$

and slip transfer was likely when *LRB* was close to 1, indicating good alignment between the slip planes at the GB and a small magnitude of the residual Burgers vector left at the grain boundary,  $\Delta b_{\alpha\beta} = |\mathbf{b}_\alpha - \mathbf{b}_\beta|$ .

Another criterion for slip transmission was proposed by Luster and Morris (1995), who emphasized the importance of the good alignment between the incoming and outgoing slip systems as well as a small magnitude of the residual Burgers vector left at the grain boundary through the geometric compatibility factor  $m'_{\alpha\beta}$ , defined as

$$m'_{\alpha\beta} = \cos \psi \cos \kappa. \quad (3)$$

Slip transfer was likely when  $m'_{\alpha\beta}$  was close to 1, as it indicates full compatibility between the slip systems  $\alpha$  and  $\beta$  across the GB because both the slip directions and the slip planes are parallel and dislocations should be easily transmitted across the GB. On the contrary, the slip systems are incompatible if  $m'_{\alpha\beta} = 0$  because either the slip directions or slip planes are orthogonal. This criterion has been used to assess slip transfer and blocking across GBs in various investigations. For instance, Hémerly et al. (2018) studied slip transfer in Ti-6Al-4V alloy polycrystals and found that high values of  $m'_{\alpha\beta}$ , combined with high resolved shear stress in the outgoing slip system, was a good indicator of the probability of slip transfer. Bieler et al. (2019) and Alizadeh et al. (2020) analyzed slip transfer in over 250 grain boundaries in pure Al polycrystals and concluded that slip transfer is likely to occur when  $m'_{\alpha\beta} > 0.9$  and  $\Delta b_{\alpha\beta} < 0.35|\mathbf{b}|$ , or at values of  $m'_{\alpha\beta}/\Delta b_{\alpha\beta}$  that exceed a threshold. Finally, Abuzaid et al. (2016) also concluded the small values of  $\Delta b_{\alpha\beta}$  are also good indicators of slip transfer. Zhao et al. (2020) analyzed these experimental data using artificial neural networks to conclude that op-

imum predictions of slip transfer (with an accuracy close to 90%) can be achieved through the combination of two geometrical metrics (such as GB misorientation and  $m'_{\alpha\beta}$ ).

The effect of these geometrical criteria on slip transfer was recently included in a physically-based crystal plasticity model that was used to study stress concentrations in either transparent, translucent or opaque GBs in bicrystals oriented for single and double slip (Haouala et al., 2020a). The results of the numerical simulations were in good agreement with experimental observations of slip transfer and slip activation on Al GBs, indicating that the crystal plasticity model was able to capture the effect of GBs on the slip behavior of FCC polycrystals. This strategy is extended in this paper to determine the flow strength of different FCC polycrystals by means of computational homogenization of an RVE of the microstructure, leading to accurate predictions of the Hall-Petch effect in Al, Cu, Ni and Ag particularly for grain sizes  $< 20 \mu\text{m}$ . Moreover, the influence of the GB character (either transparent, translucent or opaque) on the local stresses that may trigger damage is also highlighted.

## 2. Physically-based crystal plasticity model

The mechanical behavior of the single crystals in the polycrystal is governed by a physically-based, rate-dependent crystal plasticity model (Haouala et al., 2018), which was modified to include the effect of slip blocking or transfer between slip systems concurring at a GB (Haouala et al., 2020a). The model was developed within the framework of finite deformations using the multiplicative decomposition of the deformation gradient, following standard crystal plasticity implementations (Segurado et al., 2018).

The relationship between the plastic shear deformation rate in the slip system  $\alpha$ ,  $\dot{\gamma}^\alpha$ , and the corresponding resolved shear stress,  $\tau^\alpha$ , is expressed by

$$\dot{\gamma}^\alpha = \dot{\gamma}_0 \left( \frac{|\tau^\alpha|}{\tau_c^\alpha} \right)^{\frac{1}{m}} \text{sgn}(\tau^\alpha) \quad (4)$$

where  $\dot{\gamma}_0$  is the reference shear strain rate,  $m$  the strain rate sensitivity parameter and  $\tau_c^\alpha$  is the critical resolved shear stress (CRSS) in the slip system

$\alpha$ . Standard values of  $\gamma_0$  and  $m$  for FCC polycrystals can be found in Table 1 (Haouala et al., 2018).

The evolution of the CRSS during deformation follows a particularization of the Taylor model (Taylor, 1934) by Franciosi et al. (1980) which includes the contribution between dislocations in different slip systems to the hardening according to

$$\tau_c^\alpha = \mu b \sqrt{\sum_{\delta} q^{\alpha\delta} \rho^\delta} \quad (5)$$

where  $\mu$ ,  $b$  and  $\rho^\delta$  stand for the shear modulus parallel to the slip plane, the Burgers vector and the dislocation density in slip system  $\delta$ , respectively. The dimensionless coefficients  $q^{\alpha\delta}$  stand for the different interactions between pairs of slip systems and were obtained by means of discrete dislocation dynamics simulations for FCC lattices where dislocation slip occurs in 12  $\{111\}\langle 110 \rangle$  systems (Devincre et al., 2008; Bertin et al., 2013). Due to symmetry considerations, only six independent coefficients are necessary to determine the  $12 \times 12$  coefficients of  $q^{\alpha\delta}$  and they are depicted in Table 1.

The evolution of the dislocation density in each slip system,  $\dot{\rho}^\alpha$ , follows the Kocks-Mecking law (Kocks et al., 1979; Kocks and Mecking, 2003) that takes into account the balance between the generation and annihilation of dislocations. Nevertheless, the original idea of Kocks-Mecking was modified by Haouala et al. (2020a) to account for the formation of dislocation pile-ups in the slip system near a GB that does not allow for slip transfer leading to

$$\dot{\rho}^\alpha = \frac{1}{b} \left( \frac{1}{\ell^\alpha} - 2y_c \rho^\alpha \right) |\dot{\gamma}^\alpha| \quad \text{if slip transfer is allowed for any } \beta \quad (6)$$

$$\dot{\rho}^\alpha = \frac{1}{b} \left( \max \left( \frac{1}{\ell^\alpha}, \frac{K_s}{d_b} \right) - 2y_c \rho^\alpha \right) |\dot{\gamma}^\alpha| \quad \text{if slip transfer is blocked } \forall \beta \quad (7)$$

where  $\beta$  stands for any slip system in the nearest neighbor grain. Eq. (6) stands for the standard Kock-Mecking law that includes two terms that control the generation and annihilation of dislocations. Dislocation generation in the slip system  $\alpha$  depends on the dislocation Mean Free Path (MFP),  $\ell^\alpha$ , which stands for the distance travelled by a dislocation segment before it is

Table 1: Parameters of the dislocation-based crystal plasticity model for FCC single crystals.

<i>Viscoplastic parameters</i>	
Reference shear strain rate $\dot{\gamma}_0$ ( $s^{-1}$ )	$10^{-4}$
Strain rate sensitivity coefficient $m$	0.05
<i>Dislocation interaction coefficients (<math>q^{\alpha\delta}</math>)</i>	
Self interaction	0.122
Coplanar interaction	0.122
Collinear interaction	0.657
Glissile junction	0.137
Hirth lock	0.084
Lomer-Cottrell lock	0.118

stopped by an obstacle and it is given by

$$l^\alpha = \frac{K}{\sqrt{\sum_{\delta \neq \alpha} \rho^\delta}} \quad (8)$$

where  $\rho^\delta$  is the dislocation density in the slip system  $\delta$  and  $K$  is a dimensionless constant, known as the similitude coefficient, that relates the flow stress with the average wavelength of the characteristic dislocation pattern. It was estimated by Sauzay and Kubin (2011) and Rubio et al. (2019) for different FCC polycrystals. Dislocation annihilation is controlled by current dislocation density in the system  $\alpha$  and  $y_c$ , the effective annihilation distance between dislocations. This latter parameter was estimated for different FCC metals by Rubio et al. (2019) assuming equal densities of edge and screw dislocations. The annihilation distance for edge dislocations is very small ( $\approx 6b$ ) and independent of the metal while that for screw dislocations is a function of the stacking fault energy (Essmann and Mughrabi, 1979; Kubin, 2013). Eq. (6) establishes the dislocation accumulation rate at any slip sys-



tem in any Gauss point of the polycrystal that is either far away from any GB boundary or when -even if the Gauss point is close to a GB- slip transfer to another slip system  $\beta$  is possible across the GB according to a geometrical criteria that has to be defined.

In contrast, Eq. (7) provides the dislocation accumulation rate for a slip system at a Gauss point near a GB when slip transfer across the boundary is blocked according to the geometrical criteria. The critical distance at the GB that leads to an increase in the dislocation generation rate (and, thus, to the formation of a dislocation pile-up) is given by the condition  $K_s/d_b > 1/\sqrt{\ell^\alpha}$  where  $K_s$  is another dimensionless constant that determines the storage of dislocations at the GB and  $d_b$  is the distance from the Gauss point to the nearest GB along the slip direction.  $K_s$  was also determined by means of 3D dislocation dynamics simulations in the presence of impenetrable grain boundaries in FCC polycrystals (De Sansal et al., 2010) while  $d_b$  depends on the location of the Gauss point and on the orientation of the crystal. The different coefficients of the crystal plasticity model for FCC Al, Ni, Cu and Ag as well as the elastic constants are depicted in Table 2.

### 3. Polycrystal homogenization framework

The mechanical behavior of polycrystals with different grain sizes was determined by means of the finite element simulation of the deformation of cubic RVEs of the microstructure under uniaxial tension, following the standard procedures in full-field computational homogenization (Segurado et al., 2018). To this end, RVEs containing grains with random crystallographic orientations were generated using the open-source software Neper (Quey et al., 2011) and discretized with second order modified tetrahedra with *Gmsh* (Geuzaine and Remacle, 2009) (C3D10M elements with 10 nodes in Abaqus). The shape of the grains was equiaxed and the grain sizes followed a lognormal distribution with average grain size  $\bar{D}_g$  and standard deviation of  $0.2\bar{D}_g$  (Fig. 2).

The microstructure of the RVE was periodic along the three directions of the space and periodic boundary conditions were applied to all the nodes on the boundary of the domain. The displacements of each pair of nodes A and B located on opposite surfaces of the domain were linked according to

Table 2: Parameters of the dislocation-based crystal plasticity model for the FCC crystals (Haouala et al., 2018; Rubio et al., 2019)

	Cu	Al	Ni	Ag
<i>Elastic constants (GPa)</i>				
$C_{11}$	168.4	108	249	124
$C_{12}$	121.4	61.3	155	93.7
$C_{44}$	75.4	28.5	114	46.1
Shear modulus $\mu$	30.5	25.0	58.4	19.5
<i>Dislocation parameters</i>				
Burgers vector $b$ (nm)	0.256	0.286	0.250	0.288
Effective annihilation distance $y_c$ (nm)	15	56	14	12.5
Dislocation storage coefficient $K$	6	9	11	5
Grain boundary storage coefficient $K_s$	5	5	5	5

$$\mathbf{u}_B - \mathbf{u}_A = (\bar{\mathbf{F}} - \mathbf{I})L \quad (9)$$

where  $L$  is the length of the cubic domain. The far-field deformation gradient  $\bar{\mathbf{F}}$  applied to the RVE is obtained by prescribing the displacements of three master nodes  $M_i$ .

$$\mathbf{u}(M_i) = (\bar{\mathbf{F}} - \mathbf{I})\mathbf{e}_i \quad (10)$$

where  $\mathbf{e}_i$  with  $i = 1, 2, 3$  stand for the orthogonal basis along the three Cartesian axes  $x, y, z$ . The master nodes are linked to the microstructure by three springs of negligible stiffness, joined to a fixed node inside the RVE. The displacement of the master nodes is prescribed by applying a nodal force  $P_j$  to the master node  $M_i$  and degree of freedom  $j$  according to

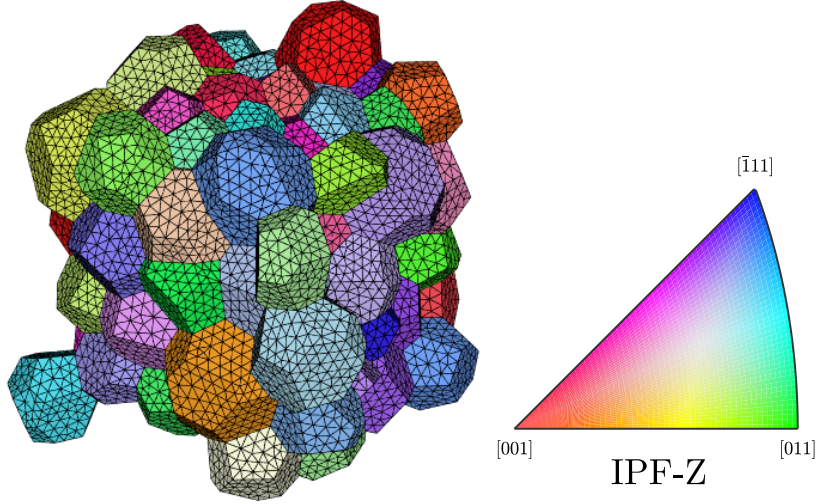


Figure 2: RVE of the microstructure including 100 grains discretized with 150000 second order tetrahedra. The colour of each grain corresponds to the orientation with respect to the Z axis as indicated in the inverse pole figure.

$$P_j(M_i) = (\bar{\sigma} \mathbf{e}_i)_j A_i \quad (11)$$

where  $\bar{\sigma}$  is the far-field stress tensor and  $A_i$  is the projection of the current area of the face perpendicular to the  $\mathbf{e}_i$  in this direction.

In order to apply eqs. (6) and (7), it is necessary to calculate the distance  $d_b$  from each Gauss integration point to the nearest GB along the slip direction corresponding to each slip system and to identify the grain across the boundary. This latter information is necessary to apply the geometrical criteria ( $LRB$ ,  $m'_{\alpha\beta}$ ,  $\Delta b$  or any combination thereof) to assess whether slip transfer across the GB is possible for each slip system. This information only depends on the geometry of the RVE and the discretization and the values of  $d_b$  for each slip system in each Gauss point are calculated and stored before the numerical analysis. The strategy to determine  $d_b$  is schematically presented in Figure 3, which shows a simplified 2D representation of a section of a polycrystal in which grain A is surrounded by grains B, C and D. The integration point  $P_0$  that belongs to a tetrahedral element of grain A (shaded in grey) is plotted in green in Fig. 3 and the slip direction corresponding to the slip system  $\alpha$  is plotted as a dashed blue line. The first step

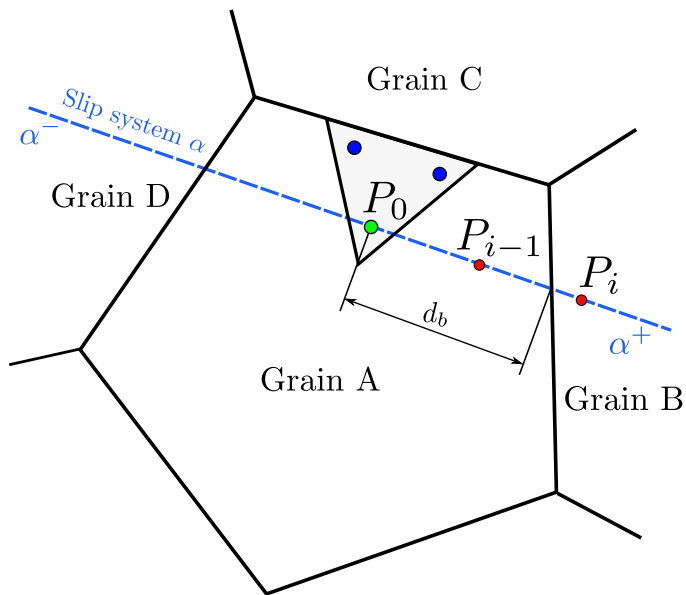


Figure 3: Schematic of the calculation of the distance from a Gauss point to the nearest GB along one slip direction.

to calculate the distance  $d_b$  is to identify positions  $P_0$  to  $P_1$  along the positive slip direction (indicated by  $\alpha^+$  in the figure) using the distance  $0.5R_{eq}$ , where  $R_{eq}$  is the equivalent grain A radius (determined from the volume of the grain assuming that it is spherical). If  $P_1$  belongs to grain A (which is easily determined from the coordinates of the vertices of grain A, which is a convex polyhedron), the process is repeated until the position of  $P_i$  is outside of grain A and within grain B. Then, a bisection method is used to determine the position of the GB between  $P_i$  and  $P_{i-1}$  with a given tolerance and to determine  $d_b$  along the positive slip direction. The same procedure is repeated for the negative slip direction and the corresponding distance to the opposite GB as well as the grain across this boundary is determined (grain D in this case). The minimum value of  $d_b$  from both directions is stored as  $d_b$  together with the identifier for the nearest neighbor grain. It was assumed that  $d_b$  is constant throughout the analysis, a reasonable assumption because of the small applied far-field strain in the simulations (5%).

An exception appears when the integration point is lying next to the outer boundary of the RVE because a point  $P_i$  outside the RVE does not lie in the convex hull of any grain. In this case, the grain across the boundary along

any slip system has to be determined taking into account the periodicity of the RVE. The point  $P_i$  outside the RVE is shifted in the three directions of the space by a distance  $\pm L$ . Because of the periodicity of the RVE, one of the new positions of  $P_i$  has to fall within one grain, which is the nearest neighbor along such slip system.

Once the neighbor grain across the boundary has been identified for each slip system  $\alpha$  at each Gauss integration point in grain A, the likelihood of slip transfer from the slip system  $\alpha$  in grain A to any of the slip systems  $\beta$  in the neighbor grain B can be assessed using any of the geometrical criteria detailed in the introduction. Two of them, based on the Luster-Morris geometric compatibility criterion  $m'_{\alpha\beta}$  and on the residual Burgers vector  $\Delta b_{\alpha\beta}$ , have been used in this investigation. They can be computed as (Bayerschen et al., 2016) (Fig. 1),

$$m'_{\alpha\beta} = (\mathbf{n}'_{\alpha} \cdot \mathbf{n}_{\beta})(\mathbf{b}'_{\alpha} \cdot \mathbf{b}_{\beta}) \quad \text{and} \quad \Delta b_{\alpha\beta} = |\mathbf{b}'_{\alpha} - \mathbf{b}_{\beta}| \quad (12)$$

where  $\mathbf{n}'_{\alpha}$  and  $\mathbf{n}_{\alpha}$  are unit vectors perpendicular to the slip plane  $\alpha$  in grain A and slip plane  $\beta$  in grain B. Obviously, all the vectors in eq. (12) have to be expressed in the same reference frame. The orientation of grain A with respect to the Cartesian reference frame of the RVE is given by the Euler angles  $(\varphi_1^A, \phi^A, \varphi_2^A)$  while that of grain B is given by  $(\varphi_1^B, \phi^B, \varphi_2^B)$ . The vectors  $\mathbf{n}'_{\alpha}$  and  $\mathbf{b}'_{\alpha}$  expressed in the reference frame of crystal A can be transformed to the reference frame of crystal B,  $\mathbf{n}_{\alpha}$  and  $\mathbf{b}_{\alpha}$ , according to

$$\mathbf{n}_{\alpha} = \mathbf{n}'_{\alpha} \mathbf{G}_A^{-1} \mathbf{G}_B \quad \text{and} \quad \mathbf{b}_{\alpha} = \mathbf{b}'_{\alpha} \mathbf{G}_A^{-1} \mathbf{G}_B \quad (13)$$

where  $\mathbf{G}_A$  and  $\mathbf{G}_B$  stand for the orientation matrices of grains A and B, where, again, orientations are expressed with respect to the Cartesian reference frame of the RVE as a function of the Euler angles of each grain according to (Schwartz et al., 2009)

$$\mathbf{G} = \begin{pmatrix} \cos \varphi_1 \cos \varphi_2 - \sin \varphi_1 \sin \varphi_2 \cos \phi & \sin \varphi_1 \cos \varphi_2 + \cos \varphi_1 \sin \varphi_2 \cos \phi & \sin \varphi_2 \sin \phi \\ -\cos \varphi_1 \sin \varphi_2 - \sin \varphi_1 \cos \varphi_2 \cos \phi & -\sin \varphi_1 \sin \varphi_2 + \cos \varphi_1 \cos \varphi_2 \cos \phi & \cos \varphi_2 \sin \phi \\ \sin \varphi_1 \sin \phi & -\cos \varphi_1 \sin \phi & \cos \phi \end{pmatrix}.$$

Slip transfer between slip systems  $\alpha$  and  $\beta$  is allowed when  $m'_{\alpha\beta}$  is above (or  $\Delta b_{\alpha\beta}$  below) a threshold value. If the condition of slip transfer is fulfilled

for any  $\beta$  slip system in the neighbor grain, eq. (6) is used as the constitutive equation of slip system  $\alpha$  at the Gauss integration point of the crystal. Otherwise, slip transfer from  $\alpha$  to  $\beta$  is not possible due to the geometric incompatibility and the constitutive equation is expressed by eq. (7).

It should be noted that these changes in the slip behavior due to the presence of impenetrable GBs are only active near to the grain boundaries (as dictated by the condition  $K_s/d_b > 1/\sqrt{\ell^\alpha}$ ). Moreover, the geometrical analysis of slip transfer at each GB indicates how many pairs of slip systems are suitably oriented to transfer slip across the boundary, leading to a classification of GBs from fully opaque (slip transfer is not possible for any pair of slip systems) to translucent (slip transfer is possible for some pairs of slip systems) to fully transparent (slip transfer is allowed for all 12 pairs of slip systems).

The mechanical behavior of the RVEs under uniaxial tension was simulated using Abaqus/Standard Abaqus (2020) within the framework of the finite deformations theory with the initial unstressed state as reference. The constitutive behavior of each crystal was governed by the crystal plasticity model presented in Section 2, that was implemented in Abaqus through a user-defined material model (UMAT).

## 4. Results and discussion

### 4.1. Selection of RVE size and discretization

An initial set of simulations was carried out in RVEs of Cu with fully opaque GBs to assess the effect of the discretization and of the number of grains in the RVE on the calculated stress-strain curves. RVEs with 100 grains were discretized with either 12000, 150000 and 350000 C3D10M elements. The coarse discretization overestimated the flow strength of the polycrystal by  $\approx 10\%$  while the difference in flow strength between the medium and fine discretizations was only 2%. In addition, the mechanical response of RVEs with 50, 100 and 200 grains and random texture was calculated using approximately the same discretization ( $\approx 50000$  elements). The differences in the flow strength between the RVEs with 50 and 100 grains were about 5% and only of 2% between the RVEs with 100 and 200 grains. Thus, RVEs with 100 grains discretized with 150000 C3D10M elements were selected for the analysis in order to optimize the balance between time and accuracy

(Figure 2). Simulations of the same RVE with three different sets of random orientations showed differences of 4% between the maximum and minimum flow stress. So, the texture that led to a flow stress in between the maximum and the minimum was selected for the simulations presented in this paper. This ensures that the flow stresses predicted by the different models were very close to the mean obtained by averaging the results of different RVEs and that the maximum differences from this mean value should be  $< 2\%$  regardless of the particular random grain orientation distribution in the RVE.

#### 4.2. Effect of slip transfer on the flow strength

The effect of grain size and grain boundary character on the mechanical response of Al and Cu polycrystals was analyzed using the crystal plasticity model and the computational homogenization scheme presented above. To this end, RVEs with four different grain sizes  $\bar{D}_g$  (10, 20, 40 and 80  $\mu\text{m}$ ) and the same set of randomly-generated orientations were generated. Simulations were performed at quasi-static strain rates ( $\approx 10^{-3} \text{ s}^{-1}$ ) under uniaxial tension up to 5% applied strain. The initial dislocation density was  $\approx 10^{12} \text{ m}^{-2}$ , evenly distributed among the 12 slip systems, which corresponds to well-annealed polycrystals. The parameters of the crystal plasticity model for both Al and Cu can be found in Tables 1 and 2.

The effect of grain boundary character on the engineering stress-strain curves in tension of Al and Cu polycrystals with different average grain sizes ( $\bar{D}_g = 10 \mu\text{m}$  and  $40 \mu\text{m}$ ) is presented in Figs. 4a to d. The stress in these plots has been normalized by  $\mu b$  to reveal the differences in strain hardening between Al and Cu as a result of the interaction, accumulation and annihilation of dislocations and to compensate for the effect of the differences in elastic constants. Five different curves are plotted in each figure: the strongest polycrystals correspond to simulations in which all GBs are assumed to be opaque and, thus, the constitutive equation of the material is given by eq. (7). In contrast, the softest response is given by the dashed black curves that were obtained assuming that all GBs were fully transparent. The constitutive equation of the polycrystal in this case is given by eq. (6) and the results of the simulations are independent of  $\bar{D}_g$  and stand for the behavior of a polycrystal with an "infinite" grain size. Obviously, the differences in the flow stress between polycrystals with fully opaque and fully transparent GBs increase as the average grain size decreases, in agreement with the Hall-Petch effect. It should be noted that the stress-strain

curves of Al polycrystals with either opaque or transparent GBs in Figs. 4a and b show very little strain hardening for strains  $> 2\%$  and this behavior is associated with the high values of  $K$  and  $y_c$  in the constitutive model. Dislocation multiplication is responsible for the strain hardening in the bulk crystals, and decreases as the similitude coefficient  $K$  increases because the dislocation MFP is proportional to  $K$ . Moreover, dislocation annihilation -which reduces the strain hardening- is more efficient for higher  $y_c$ . In contrast, the stress-strain curves of Cu polycrystals present continuous strain hardening because  $K$  and  $y_c$  are smaller. Thus, Al and Cu represent two FCC polycrystals with very different strain hardening properties.

The three curves between those corresponding to fully opaque and fully transparent GBs in Figs. 4a to d show the behavior of polycrystals where slip transfer is allowed between slip systems that intersect at a GB when the Luster-Morris parameter  $m'_{\alpha\beta}$  is higher than a threshold given by 0.9, 0.75 or 0.5. The higher the threshold, the closer the stress-strain curves are to the fully-opaque case. On the other hand, the stress-strain curves obtained with a threshold  $m'_{\alpha\beta} > 0.5$  are almost the same as those obtained with fully-transparent GBs for both Al and Cu. The effect of slip transfer on the formation of dislocation pile-ups near the GBs can be ascertained from the spatial distribution plots of the dislocation density in a cross-section of the RVEs corresponding to Al (Figs. 5a, c and e) and Cu polycrystals (Fig. 5b, d and f) with an average grain size of  $10 \mu\text{m}$  deformed up to 5%. Obviously, high dislocation densities are found at all of GBs if they are assumed to be opaque (Figs. 5a and b), leading to a large increase in the flow stress observed in Figs. 4a and c for Al and Cu polycrystals with  $\bar{D}_g = 10 \mu\text{m}$ . As slip transfer is allowed, some opaque GBs become translucent or transparent as slip transfer is allowed, as shown in Figs. 5c and e for Al and in d and e for Cu, and the number of GBs in which dislocation pile-ups have disappeared increases as the geometrical threshold for slip transfer is reduced in the model. In the case of  $m'_{\alpha\beta} > 0.5$  (not shown in the figure), practically all GBs are transparent and no dislocation pile-ups can be found.

The formation of pile-ups at GBs is directly associated with an increase in the local stresses, as shown in the spatial distribution plots of the Von Mises stress in the cross-section of the RVEs of Al (Fig. 6a, c and e) and Cu polycrystals (Fig. 6b, d and f) with an average grain size of  $10 \mu\text{m}$  deformed up to 5%. The more transparent the GB, the lower the stress concentration and, thus, slip transfer is likely to play a dominant role on the determination



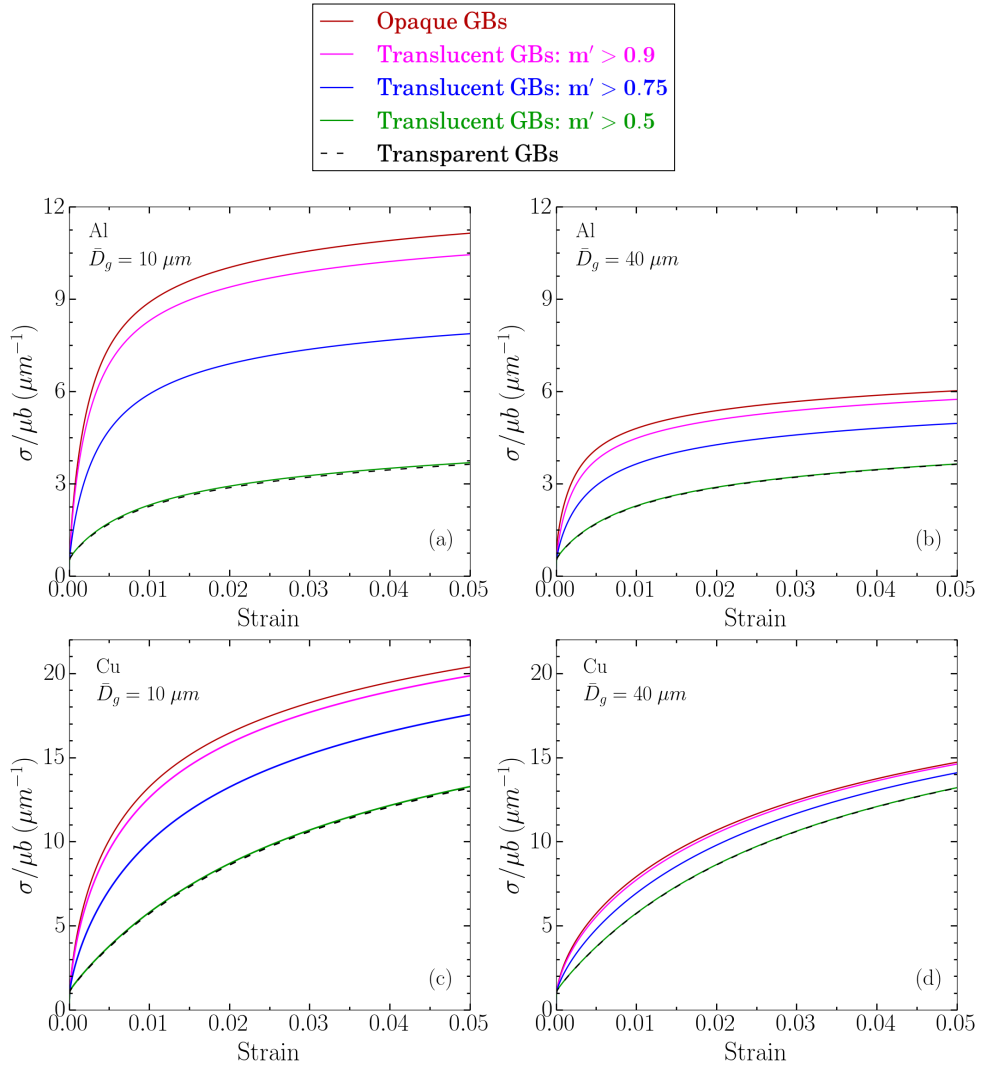


Figure 4: Engineering stress-strain curves of Al and Cu polycrystals as a function of grain boundary type: (a) Al  $\bar{D}_g = 10 \mu\text{m}$ , (b) Al  $\bar{D}_g = 40 \mu\text{m}$ , (c) Cu  $\bar{D}_g = 10 \mu\text{m}$  and (d) Cu  $\bar{D}_g = 40 \mu\text{m}$ .

of the GBs at which damage is likely to develop in polycrystals.

The results presented above show how slip transfer influences the local dislocation density and flow stress at GBs. Obviously, the reduction in the strength of the polycrystal should be related to the threshold for translucent

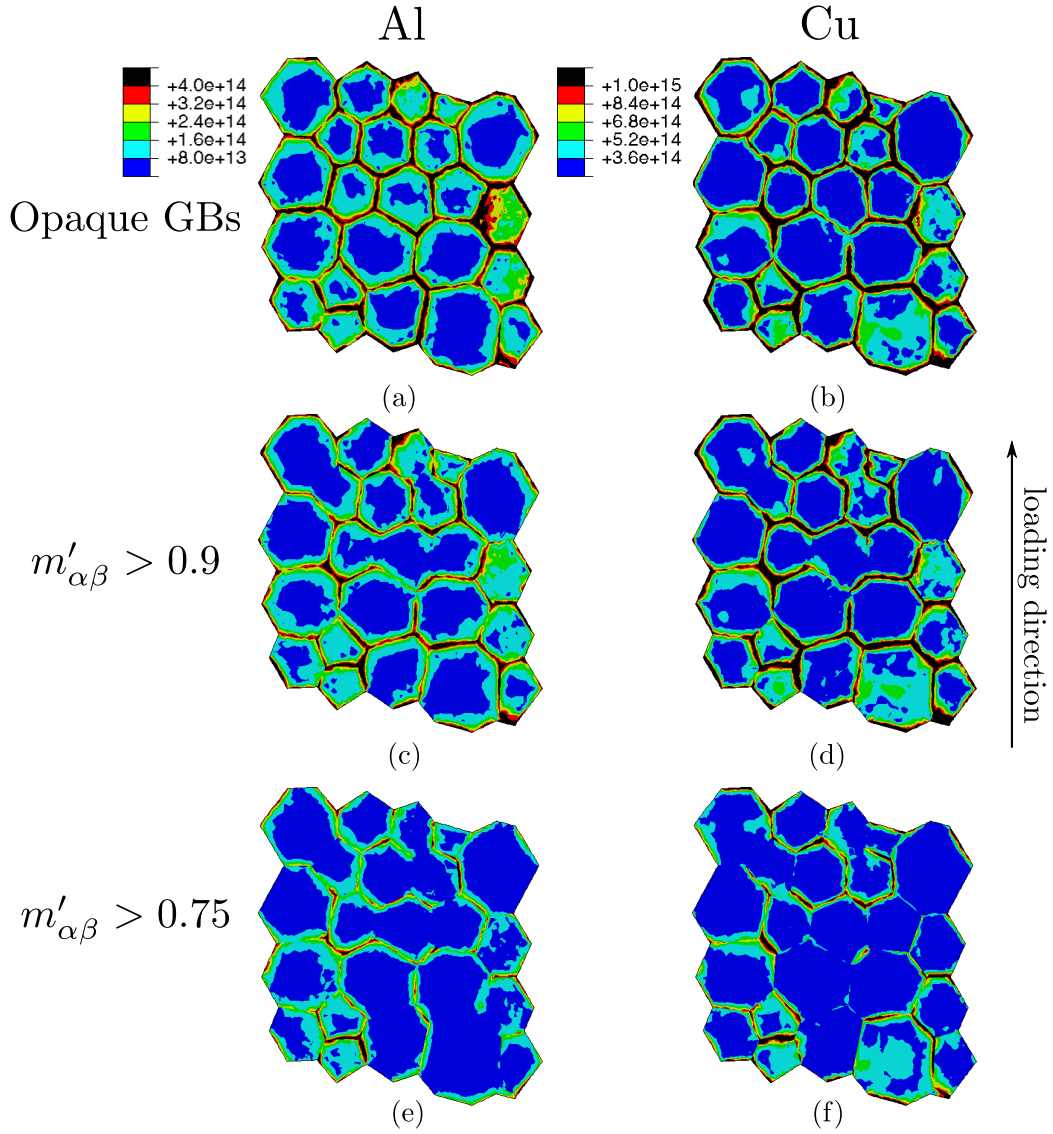


Figure 5: Spatial distribution of the total dislocation density (in  $m^{-2}$ ) in a cross-section of the RVE of the Al and Cu polycrystals with an average grain size of  $10 \mu m$  deformed up to 5%. (a) Al, opaque GBs. (b) Cu, opaque GBs. (c) Al, translucent GBs with  $m'_{\alpha\beta} > 0.9$ . (d) Cu, translucent GBs with  $m'_{\alpha\beta} > 0.9$ . (e) Al, translucent GBs with  $m'_{\alpha\beta} > 0.75$ . (f) Cu, translucent GBs with  $m'_{\alpha\beta} > 0.75$ .

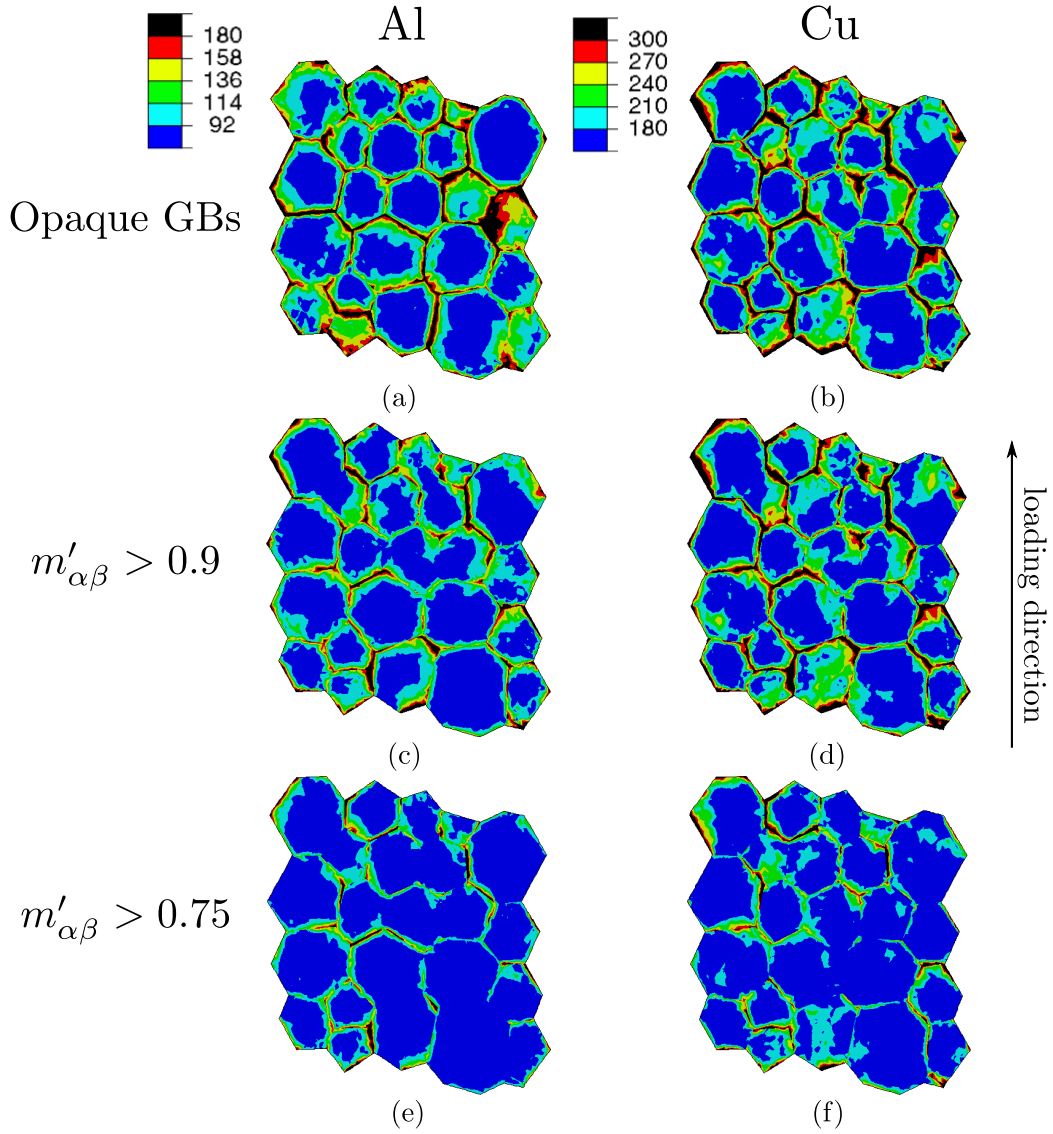


Figure 6: Spatial distribution of the Von Mises stress (in MPa) in a cross-section of the RVE of the Al and Cu polycrystals with an average grain size of  $10 \mu\text{m}$  grain size deformed up to 5%. (a) Al, opaque GBs. (b) Cu, opaque GBs. (c) Al, translucent GBs with  $m'_{\alpha\beta} > 0.9$ . (d) Cu, translucent GBs with  $m'_{\alpha\beta} > 0.9$ . (e) Al, translucent GBs with  $m'_{\alpha\beta} > 0.75$ . (f) Cu, translucent GBs with  $m'_{\alpha\beta} > 0.75$ .

GBs in the RVE. This information can be obtained from the geometrical analysis to determine the nearest neighbor grain for each slip system  $\alpha$  presented in section 3 and the corresponding  $m'_{\alpha\beta}$  values for all the  $\beta$  slip systems in the nearest neighbor grain. Then, a GB between grains A and B is characterized from the viewpoint of slip transfer by all the  $m'_{\alpha\beta}$  values between all the slip systems in grains A and B. The translucency of the grain boundary can be assessed by analyzing the number of slip systems that fulfil a slip transfer criterion. Taking into account that FCC crystals have 12 slip systems from the  $\{111\} \langle 110 \rangle$  family, a  $12 \times 12$   $m'_{\alpha\beta}$  matrix is calculated for pairs of neighbor grains, where each row relates the geometric compatibility of the lattice from a given incoming slip system  $\alpha$ . In this context, slip transfer is considered possible along a certain slip system, for instance  $\alpha = 1$ , when any of the  $m'_{1\beta}$  values for the 12 possible outgoing slip systems  $\beta$  in the nearest neighbor grain is above the threshold for slip transfer. Thus, the number of slip systems in grain A that can transfer slip can be determined for each grain boundary and the grain boundaries in the RVE can be classified according to their translucency to dislocations in three distinct groups: opaque GBs (slip transfer is not allowed for any pair of slip systems), translucent or partially-transparent GBs (slip transfer is allowed along several pairs of slip systems) and fully transparent GBs (slip transfer is allowed in all slip systems).

The fraction of GBs in the RVE as a function of the number of transparent slip systems across the boundary is plotted in Figs. 7a to c for different values of the threshold  $m'_{\alpha\beta}$  for slip transfer. If the threshold for slip transfer is very high,  $m'_{\alpha\beta} > 0.9$  (Fig. 7a), 48% of the GBs are fully opaque while only 3.4% of the GBs are fully transparent (all slip systems in one grain can transfer slip to -at least- one slip system in the neighbor grain). Most of the remaining slip systems are translucent and contain 1 to 4 slip systems that can transfer slip to the neighbor grain. The number of GBs where 5 to 11 slip systems can transfer slip is negligible. When the threshold for slip transfer is reduced to  $m'_{\alpha\beta} > 0.75$ , the fraction of fully opaque GBs drops to  $< 1\%$  while the number of fully transparent GBs increases to 11.5%. Moreover, most of the GBs can transfer slip across the GB along 4 or more slip systems. Finally, if the threshold for slip transfer is further reduced to  $m'_{\alpha\beta} > 0.5$  (Fig. 7c), almost 60% of the GBs are fully transparent and the remaining ones can transfer slip along many slip systems, leading to a polycrystal in which the effect of GBs on the strength can be neglected.

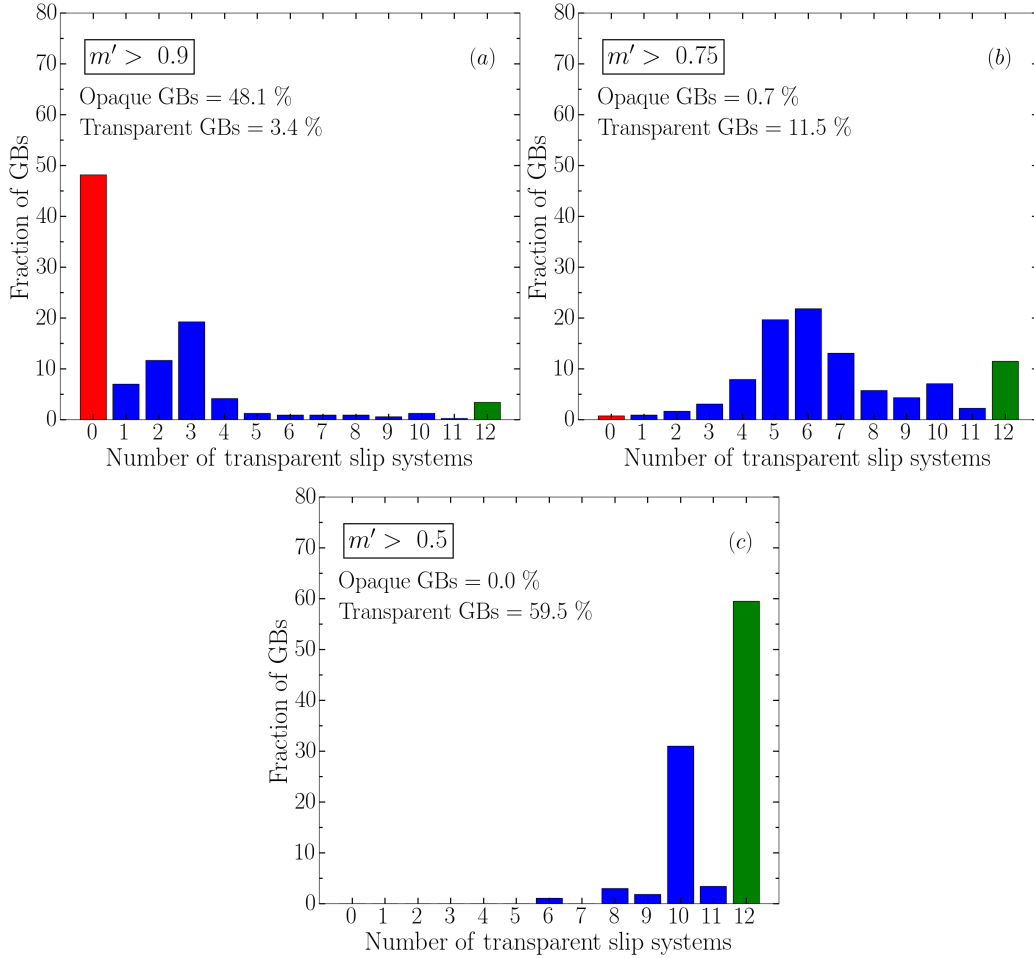


Figure 7: Fraction of GBs in the RVE as a function of the number of transparent slip systems. (a)  $m'_{\alpha\beta} > 0.9$ . (b)  $m'_{\alpha\beta} > 0.75$ . (c)  $m'_{\alpha\beta} > 0.5$ .

So far, slip transfer in the simulations has been characterized by the Luster-Morris compatibility factor but any other geometrical factor can be used in the model. For instance, the engineering stress-strain curves for Al and Cu polycrystals with an average grain size of  $10 \mu\text{m}$  are plotted in Figs. 8a and b, respectively, when slip transfer across the GB was allowed when the residual Burgers vector  $\Delta b_{\alpha\beta} < 0.45b$ . The curves corresponding to fully opaque and fully transparent GBs (as well as those obtained with a slip transfer threshold defined by  $m'_{\alpha\beta} > 0.75$ ) are also plotted for comparison. It is worth noting

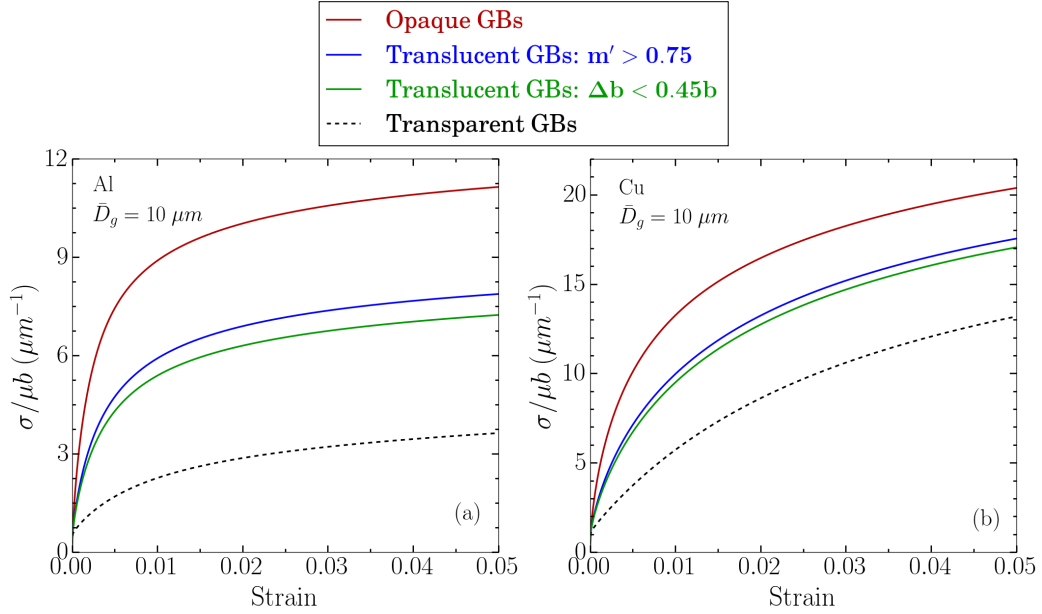


Figure 8: Engineering stress-strain curves of polycrystals with an average grain size of  $10 \mu\text{m}$  for opaque and transparent GBs as well as slip transfer criteria of  $m'_{\alpha\beta} > 0.75$  or  $\Delta b_{\alpha\beta} < 0.45b$ . (a) Al. (b) Cu.

that the stress-strain curves corresponding to  $m'_{\alpha\beta} > 0.75$  and  $\Delta b_{\alpha\beta} < 0.45b$  are almost the same for both Al and Cu, suggesting that the reduction in the flow stress due to slip transfer is mainly controlled by the fraction of opaque, translucent and transparent GBs and not by the particular criterion used. This assumption is confirmed by the histograms of the different types of GBs in the RVE from the viewpoint of slip transfer plotted in Fig. 9 for both slip transfer thresholds. The fraction of fully opaque and fully transparent GBs is very similar in both cases and most of the GBs are translucent. Thus, slip transfer is allowed in a wide number of slip systems (from 2 to 10) for both slip transfer thresholds. It is interesting to notice that pairs of slip systems of an FCC crystal share the same Burgers vectors and, thus, the number of transparent or opaque slip systems in the case of the residual Burgers vector criterion is always an even number.

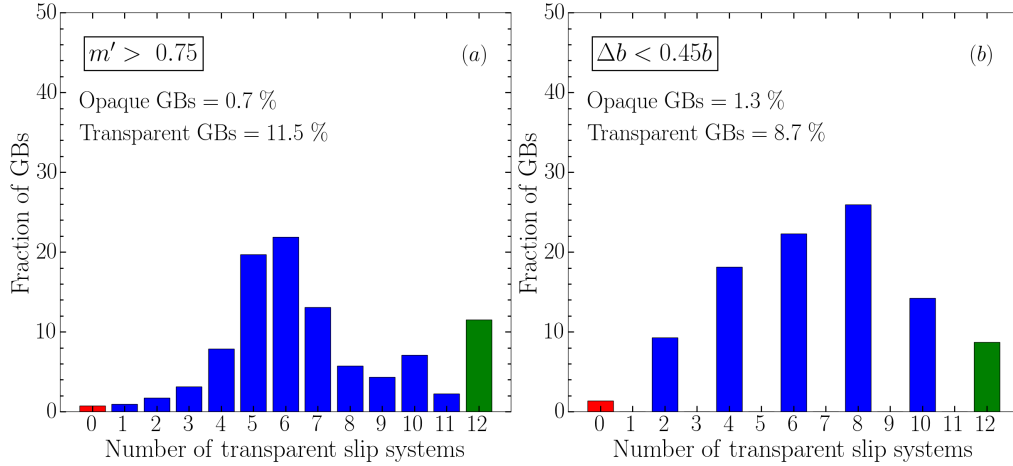


Figure 9: Fraction of GBs in the RVE as a function of the number of transparent slip systems. (a)  $m'_{\alpha\beta} > 0.75$ . (b)  $\Delta b_{\alpha\beta} < 0.45b$ .

#### 4.3. Effect of slip transfer on the Hall-Petch law

The experimental evidence indicates that the strength of polycrystals increases as the grain size decreases following a power-law of the grain size. Based on theoretical results (Zaiser and Sandfeld, 2014) and on dislocation dynamics simulations (El-Awady, 2015), the strengthening caused by GBs,  $\sigma_y - \sigma_\infty$ , has been proposed to scale with the average grain size  $\bar{D}_g$  and the square root of the initial dislocation density in the polycrystal  $\sqrt{\rho_i}$  according to (Haouala et al., 2018)

$$\sigma_y/\sigma_\infty - 1 = C(\bar{D}_g\sqrt{\rho_i})^{-x} \quad (14)$$

where  $\sigma_y$  is the flow strength of the polycrystal,  $\sigma_\infty$  the flow stress of a polycrystal with "infinite" grain size and  $C$  and  $x$  are material constants that depend on the physical parameters of the model for each FCC metal, mainly the similitude constant  $K$  and the effective annihilation distance  $y_c$ . Eq. (14) was in very good agreement with results of the simulations for Al, Cu, Ni and Ag FCC polycrystals under the assumption that all GBs were opaque (Rubio et al., 2019) leading to similar values of the exponent (in the range 0.7 to 0.9) when the applied strain was 1%. The effect of slip transfer on the flow strength of Al and Cu polycrystals with different grain size (in the range 10  $\mu\text{m}$  to 80  $\mu\text{m}$ ) deformed up to  $\varepsilon = 1\%$  and 5% is plotted in Fig 10. The initial

dislocation density in all cases was of the order of  $10^{12} \text{ m}^{-2}$ . The results of the simulations show that slip transfer reduces the strengthening provided by GBs but does not modify the exponent of eq. (14) when values of the threshold  $m'_{\alpha\beta}$  for slip transfer are similar to those reported experimentally (Hémery et al., 2018; Alizadeh et al., 2020; Zhao et al., 2020). The exponent depends on the FCC metal and on the applied strain. It is slightly lower (more negative) for Cu than for Al and decreases in both cases when the strain to determine the flow strength of the polycrystal is increased from 1% to 5% due to the effect of annihilation of dislocations near the GBs where the dislocation density is maximum. Moreover, the reduction in GB strengthening for Al is always higher than that for Cu when the thresholds for slip transfer are set to  $m'_{\alpha\beta} > 0.9$  or  $m'_{\alpha\beta} > 0.75$  although the differences are not huge. They can be attributed to changes in the dislocation accumulation and annihilation of dislocations near the GBs as a result of the differences in the physical parameters that control these phenomena in each metal.

#### 4.4. Comparison with experiments

In order to assess the validity of the modelling strategy presented above, numerical simulations of the flow stress as a function of the grain size were carried out for Al, Cu, Ni, and Ag polycrystals and compared with experimental data in the literature (Hansen, 1977; Narutani and Takamura, 1991; Carreker, 1957; Hansen and Ralph, 1982). The experiments in the literature were carried out at room temperature under quasi-static loading conditions and, therefore, the effect of the strain rate on the flow stress was considered negligible. Due to the lack of information about the initial experimental dislocation density, it was assumed to be of the order of  $10^{12} \text{ m}^{-2}$  in all cases, which is a typical value for well-annealed polycrystals. The parameters of the crystal plasticity model for Al, Cu, Ni, and Ag were obtained by Rubio et al. (2019) and can be found in Tables 1 and 2. All the simulations were carried out using the RVE shown in Fig. 2 with random texture and average grain sizes in the range  $10 \text{ }\mu\text{m}$  to  $80 \text{ }\mu\text{m}$ .

The experimental results of the flow stress in tension are plotted as a function of the inverse of the average grain size,  $\bar{D}_g^{-1}$  in Figs. 11a, b, c and d for Al, Cu, Ni, and Ag polycrystals, respectively. Data for two different strain values are shown in each figure. Two simulation results assuming fully opaque GBs (open red circles) and translucent GBs with a threshold in the Luster-Morris parameter (open blue circles) are compared. The thresholds selected for  $m'_{\alpha\beta}$



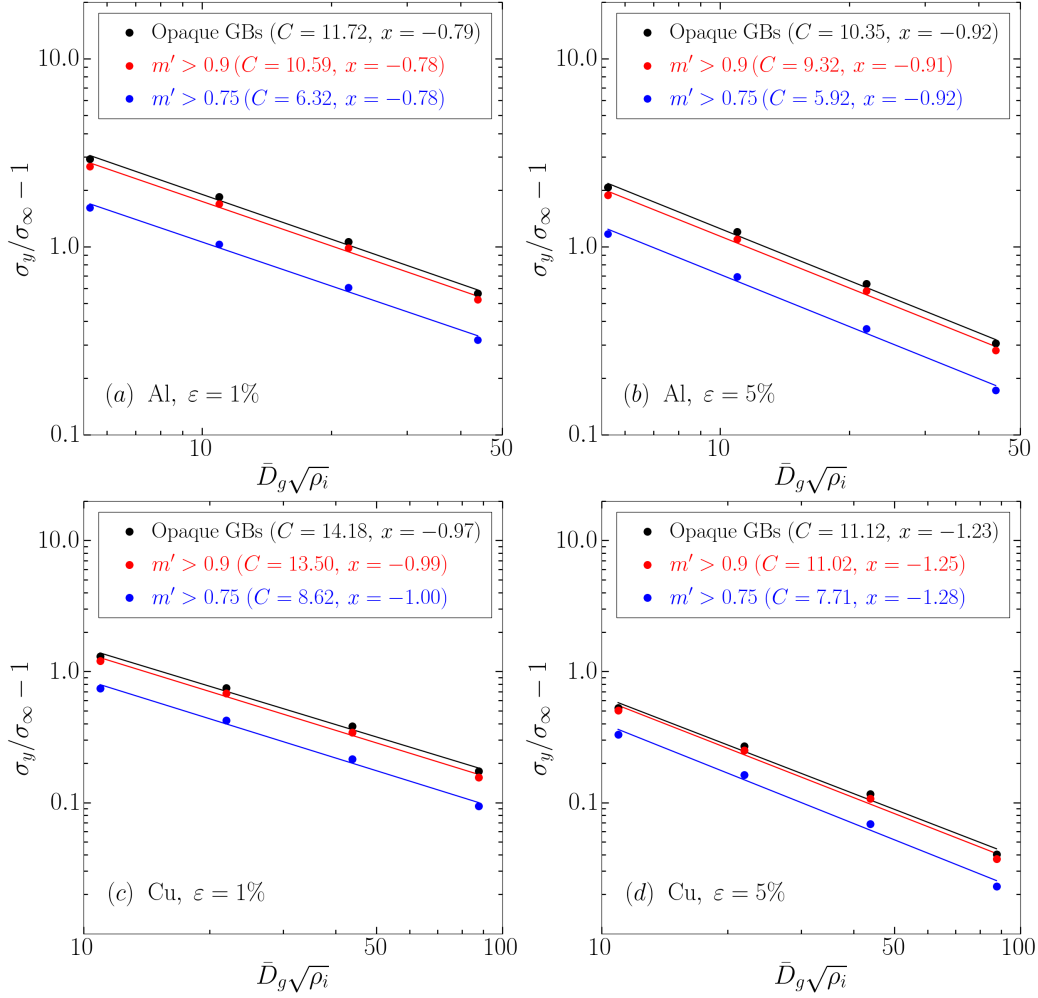


Figure 10: Grain boundary strengthening in Al and Cu polycrystals as a function of the adimensional parameter  $\bar{D}_g\sqrt{\rho_i}$ . (a) Al,  $\epsilon = 1\%$ . (b) Al,  $\epsilon = 5\%$ . (c) Cu,  $\epsilon = 1\%$ . (d) Cu,  $\epsilon = 5\%$ . The results of the simulations with fully opaque GBs and with thresholds  $m'_{\alpha\beta} > 0.9$  and  $m'_{\alpha\beta} > 0.75$  for slip transfer are plotted in each figure.

were chosen for each alloy to get a best fit of the experimental data because accurate experimental information is not available. Nevertheless, they are in the range of the values reported by different experimental investigations of slip transfer (Hémery et al., 2018; Alizadeh et al., 2020; Zhao et al., 2020). More importantly, good agreement between experiments and simulations is

found when the average grain size is large ( $\bar{D}_g^{-1} < 25 \text{ mm}^{-1}$ ,  $\bar{D}_g > 40 \text{ }\mu\text{m}$ ), regardless of the inclusion of slip transfer in the simulations, but the trend of the experimental data follows the predictions of the simulations including slip transfer when the grain sizes are smaller than  $20 \text{ }\mu\text{m}$  ( $\bar{D}_g^{-1} > 50 \text{ mm}^{-1}$ ). It should be noted, however, that the experimental dataset of Ag is smaller than those of Al, Cu and Ni, and presents larger scatter in the flow stress values, especially for 0.2% applied strain. For this reason, together with the absence of information about the initial dislocation density, it is not possible to conclude that the predictions with translucent GBs are more accurate than those carried out with opaque GBs for Ag at small strains.

It is also important to notice that slip transfer not only influences the overall strength of the polycrystal but also leads to dramatic changes in the stresses at the GBs as a function of the GB orientation (Fig. 6). These differences in GBs as a function of orientation are likely to play a dominant role on the nucleation of damage by GB cracking during monotonic and cyclic deformation or in aggressive environments (McMurtrey et al., 2015; Liang et al., 2021) as well as on the development of GB sliding during creep deformation (Wei and Anand, 2004). It is obvious that the combination of the crystal plasticity model presented in this paper together with cohesive elements at the GBs (Alabort et al., 2018) would provide a novel way to explore the role of opaque, translucent and transparent GBs on the ductility, formability and forming limits of polycrystalline materials.

## 5. Conclusions

The effect slip transfer on the flow strength of FCC polycrystals has been analyzed by means of full-field computational homogenization in combination with a physically-based crystal plasticity model. The critical resolved shear stress for plastic slip in each slip system follows the modified Taylor model while the generation and annihilation of dislocations in each slip system in the bulk during deformation is described by a Kocks-Mecking law. This law is modified near the grain boundaries to discriminate between slip systems that can or cannot transfer slip across the boundary using geometrical criteria based on the orientation and activity of the slip systems of both grains near the boundary. This model leads to a classification of the grain boundaries as fully opaque (slip transfer is not possible for any slip system), fully transparent (slip transfer is possible for all slip systems) and translucent

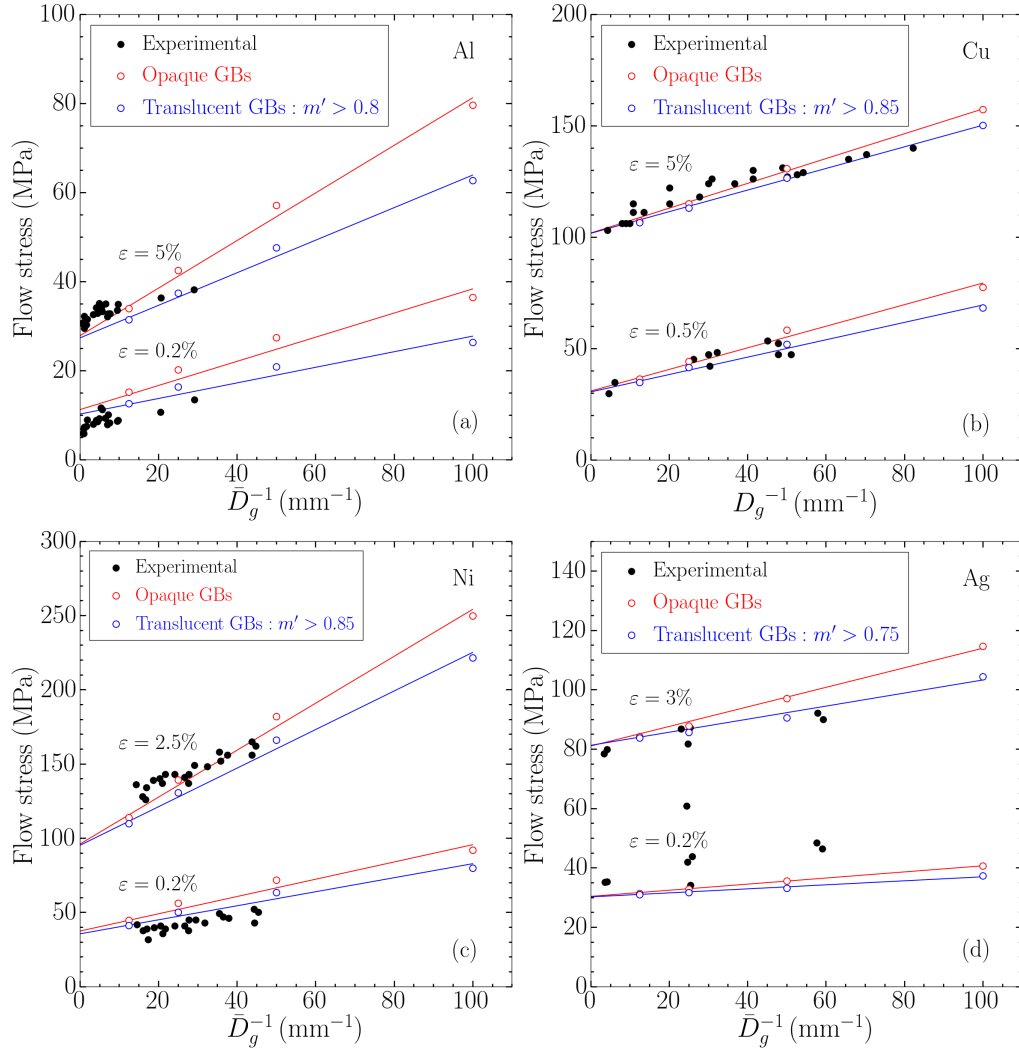


Figure 11: Experimental data from the literature and simulation results of the flow stress of Al, Cu, Ni and Ag polycrystals as a function of  $\bar{D}_g^{-1}$  for different applied strains. (a) Al. (b) Cu. (c) Ni. (d) Ag. Experimental results are indicated by black circles, while simulation results without and with slip transfer are represented by open red and blue circles.

(slip transfer is possible for several slip systems).

The mechanical behavior of Al and Cu polycrystals with grain sizes in the range  $10 \mu\text{m}$  to  $80 \mu\text{m}$  and random texture was determined assuming

that all grain boundaries were opaque, transparent or that slip transfer was possible for different thresholds of the Luster-Morris geometric compatibility parameter  $m'_{\alpha\beta}$  or of the residual Burgers vector  $\Delta b_{\alpha\beta}$ . Slip transfer between neighbor grains suitably oriented led to a clear reduction in the flow stress of the polycrystals (as compared with the simulations with opaque grain boundaries) which was dependent on the fraction of translucent and transparent grain boundaries in the microstructure, as given by the threshold in the slip transfer geometrical criterion. Moreover, dislocation densities and Von Mises stresses were much higher around opaque grain boundaries, which are potential places for damage nucleation.

The strengthening provided by grain boundaries in Al and Cu polycrystals was well described by  $C(\bar{D}_g\sqrt{\rho_i})^{-x}$  where  $\bar{D}_g$  is the average grain size and  $\rho_i$  the initial dislocation density.  $C$  depended on the material and on the fraction of translucent and transparent boundaries while  $x$  was a function of the material and of the applied strain but was independent of slip transfer at grain boundaries.

Finally, the predictions of the simulations were compared with experimental data in the literature of the effect of grain size on the strength of Al, Cu, Ni and Ag polycrystals. It was found that the inclusion of slip transfer in the model led to more accurate predictions of the Hall-Petch effect particularly for small grain sizes ( $< 20 \mu\text{m}$ ).

## Acknowledgements

This work was funded by the European Research Council Advanced Grant VIRMETAL under the European Union's Horizon 2020 research and innovation programme (Grant agreement No. 669141) and by the HexaGB project of the Spanish Ministry of Science (reference RTI2018-098245).

## References

- Abaqus, 2020. Analysis User's manual. Dassault Systèmes.
- Abuzaid, W. Z., Sehitoglu, H., Lambros, J., 2016. Localisation of plastic strain at the microstructural level in Hastelloy X subjected to monotonic, fatigue, and creep loading: the role of grain boundaries and slip transmission. *Materials at High Temperatures* 33 (4-5), 384–400.

- Acharya, A., Beaudoin, A. J., 2000. Grain size effects in viscoplastic polycrystals at moderate strains. *Journal of the Mechanics and Physics of Solids* 48, 2213–2230.
- Alabort, E., Barba, D., Sulzer, S., Libner, M., Petrinic, N., Reed, R., 2018. Grain boundary properties of a nickel-based superalloy: Characterisation and modelling. *Acta Materialia* 151, 377 – 394.
- Alizadeh, R., Peña-Ortega, M., Bieler, T. R., LLorca, J., 2020. A criterion for slip transfer at grain boundaries in Al. *Scripta Materialia* 178, 408–412.
- Ashby, M. F., 1970. The deformation of plastically non-homogeneous materials. *Philosophical Magazine* 21 (170), 399–424.
- Bargmann, S., Ekh, M., Runesson, K., Svendsen, B., 2010. Modeling of polycrystals with gradient crystal plasticity: A comparison of strategies. *Philosophical Magazine* 90, 1263–1288.
- Bayerschen, E., McBride, A. T., Reddy, B. D., Böhlke, T., 2016. Review on slip transmission criteria in experiments and crystal plasticity models. *Journal of Materials Science* 51, 2243–2258.
- Bayley, C. J., Brekelmans, W. A. M., Geers, M. G. D., 2007. A three-dimensional dislocation field crystal plasticity approach applied to miniaturized structures. *Philosophical Magazine* 87, 1361–1378.
- Bertin, N., Capolungo, L., Beyerlein, I. J., 2013. Hybrid dislocation dynamics based strain hardening constitutive model. *International Journal of Plasticity* 49, 119–144.
- Bieler, T. R., Alizadeh, R., Peña-Ortega, M., LLorca, J., 2019. An analysis of (the lack of) slip transfer between near-cube oriented grains in pure Al. *International Journal of Plasticity* 118, 269–290.
- Bieler, T. R., Eisenlohr, P., Zhang, C., Phukan, H. J., Crimp, M. A., 2014. Grain boundaries and interfaces in slip transfer. *Current Opinion in Solid State and Materials Science* 18 (4), 212–226.
- Carreker, R. P., 1957. Tensile deformation of silver as a function of temperature, strain rate, and grain size. *JOM* 9 (1), 112–115.

- Cheong, K. S., Busso, E. P., Arsenlis, A., 2005. A study of microstructural length scale effects on the behavior of FCC polycrystals using strain gradient concepts. *International Journal of Plasticity* 21, 1797–1814.
- De Sansal, C., Devincere, B., Kubin, L., 2010. Grain size strengthening in microcrystalline copper: A three-dimensional dislocation dynamics simulation. In: *Key Engineering Materials*. Vol. 423. Trans Tech Publ, pp. 25–32.
- Devincere, B., Hoc, T., Kubin, L., 2008. Dislocation mean free paths and strain hardening of crystals. *Science* 320 (5884), 1745–1748.
- Dunstan, D. J., Bushby, A. J., 2013. The scaling exponent in the size effect of small scale plastic deformation. *International Journal of Plasticity* 40, 152–162.
- Dunstan, D. J., Bushby, A. J., 2014. Grain size dependence of the strength of metals: The Hall–Petch effect does not scale as the inverse square root of grain size. *International Journal of Plasticity* 53, 56–65.
- El-Awady, J. A., 2015. Unravelling the physics of size-dependent dislocation-mediated plasticity. *Nature Communications* 6 (1), 1–9.
- Essmann, U., Mughrabi, H., 1979. Annihilation of dislocations during tensile and cyclic deformation and limits of dislocation densities. *Philosophical Magazine A* 40, 731–756.
- Franciosi, P., Berveiller, M., Zaoui, A., 1980. Latent hardening in copper and aluminium single crystals. *Acta Metallurgica* 28 (3), 273–283.
- Friedman, L. H., Chrzan, D. C., 1998. Continuum analysis of dislocation pile-ups: Influence of sources. *Philosophical Magazine A* 77, 1185–1204.
- Geuzaine, C., Remacle, J. F., 2009. Gmsh: A 3-D finite element mesh generator with built-in pre- and post-processing facilities. *International Journal for Numerical Methods in Engineering* 79 (11), 1309–1331.
- Hall, E. O., 1951. The deformation and ageing of mild steel: II Characteristics of the Lüders deformation. *Proceedings of the Physical Society. Section B* 64 (9), 742–747.

- Hansen, N., 1977. The effect of grain size and strain on the tensile flow stress of aluminium at room temperature. *Acta Metallurgica* 25 (8), 863–869.
- Hansen, N., Ralph, B., 1982. The strain and grain size dependence of the flow stress of copper. *Acta Metallurgica* 30 (2), 411–417.
- Haouala, S., Alizadeh, R., Bieler, T. R., Segurado, J., LLorca, J., 2020a. Effect of slip transmission at grain boundaries in Al bicrystals. *International Journal of Plasticity* 126, 102600.
- Haouala, S., Lucarini, S., LLorca, J., Segurado, J., 2020b. Simulation of the Hall-Petch effect in FCC polycrystals by means of strain gradient crystal plasticity and FFT homogenization. *Journal of the Mechanics and Physics of Solids* 134, 103755.
- Haouala, S., Segurado, J., LLorca, J., 2018. An analysis of the influence of grain size on the strength of FCC polycrystals by means of computational homogenization. *Acta Materialia* 148, 72–85.
- Hémery, S., Nizou, P., Villechaise, P., 2018. In situ SEM investigation of slip transfer in Ti-6Al-4V: Effect of applied stress. *Materials Science and Engineering A* 709, 277–284.
- Hirth, J. P., 1972. Influence of Grain Boundaries on Mechanical Properties. *Metall Trans* 3 (12), 3047–3067.
- Hughes, D. A., Hansen, N., Bammann, D. J., 2003. Geometrically necessary boundaries, incidental dislocation boundaries and geometrically necessary dislocations. *Scripta Materialia* 48 (2), 147–153.
- Kocks, U. F., 1970. The relation between polycrystal deformation and single-crystal deformation. *Metallurgical and Materials Transactions B* 1 (5), 1121–1143.
- Kocks, U. F., Argon, A., Ashby, M. F., 1979. The Thermodynamics and Kinetics of Slip. *Progress in Materials Science* 19, 1–291.
- Kocks, U. F., Mecking, H., 2003. Physics and phenomenology of strain hardening: The FCC case. *Progress in Materials Science* 48 (3), 171–273.
- Kubin, L., 2013. *Dislocations, Mesoscale Simulations and Plastic Flow*. Vol. 5. Oxford University Press.

- Lebensohn, R. A., Needleman, A., 2016. Numerical implementation of non-local polycrystal plasticity using Fast Fourier Transforms. *Journal of the Mechanics and Physics of Solids* 97, 333–351.
- Lee, T. C., Robertson, I. M., Birnbaum, H. K., 1989. Prediction of slip transfer mechanisms across grain boundaries. *Scripta Metallurgica* 23 (5), 799–803.
- Li, Y., Bushby, A. J., Dunstan, D. J., 2016. The Hall–Petch effect as a manifestation of the general size effect. *Proceedings of the Royal Society A* 472, 20150890.
- Liang, D., Hure, J., Courcelle, A., Shawish, S. E., Tanguy, B., 2021. A micromechanical analysis of intergranular stress corrosion cracking of an irradiated austenitic stainless steel. *Acta Materialia* 204, 116482.
- Luster, J., Morris, M. A., 1995. Compatibility of deformation in two-phase Ti-Al alloys: Dependence on microstructure and orientation relationships. *Metallurgical and Materials Transactions A* 26 (7), 1745–1756.
- McMurtrey, M., Cui, B., Robertson, I., Farkas, D., Was, G., 2015. Mechanism of dislocation channel-induced irradiation assisted stress corrosion crack initiation in austenitic stainless steel. *Current Opinion in Solid State and Materials Science* 19, 305 – 314.
- Narutani, T., Takamura, J., 1991. Grain-size strengthening in terms of dislocation density measured by resistivity. *Acta Metallurgica et Materialia* 39 (8), 2037–2049.
- Nye, J. F., 1953. Some geometrical relations in dislocated crystals. *Acta Metallurgica* 1 (2), 153–162.
- Petch, N. J., 1953. The cleavage strength of polycrystals, *Journal of Iron and Steel Institute*. *Journal of Iron and Steel Institute* 174 (1), 25–28.
- Quey, R., Dawson, P. R., Barbe, F., 2011. Large-scale 3D random polycrystals for the finite element method: Generation, meshing and remeshing. *Computer Methods in Applied Mechanics and Engineering* 200 (17-20), 1729–1745.



- Raj, S. V., Pharr, G. M., 1986. A compilation and analysis of data for the stress dependence of the subgrain size. *Materials Science and Engineering* 81, 217–237.
- Read, W. T., Shockley, W., 1950. Dislocation models of crystal grain boundaries. *Physical Review Letters* 78, 275–289.
- Rubio, R. A., Haouala, S., Llorca, J., 2019. Grain boundary strengthening of FCC polycrystals. *Journal of Materials Research* 34 (13), 2263–2274.
- Sauzay, M., Kubin, L. P., 2011. Scaling laws for dislocation microstructures in monotonic and cyclic deformation of fcc metals. *Progress in Materials Science* 56 (6), 725–784.
- Schwartz, A. J., Kumar, M., Adams, B. L., Field, D. P., 2009. *Electron backscatter diffraction in materials science*. Vol. 2. Springer.
- Segurado, J., Lebensohn, R. A., Llorca, J., 2018. Computational Homogenization of Polycrystals. *Advances in Applied Mechanics* 51, 1–114.
- Shen, Z., Wagoner, R. H., Clark, W. A., 1988. Dislocation and grain boundary interactions in metals. *Acta Metallurgica* 36 (12), 3231–3242.
- Taylor, G. I., 1934. The mechanism of plastic deformation of crystals. Part II. Comparison with observations. *Proceedings of the Royal Society of London A* 145 (855), 388–404.
- Wei, Y. J., Anand, L., 2004. Grain-boundary sliding and separation in polycrystalline metals: application to nanocrystalline fcc metals. *Journal of the Mechanics and Physics of Solids* 52, 2587 – 2616.
- Zaiser, M., Sandfeld, S., 2014. Scaling properties of dislocation simulations in the similitude regime. *Modelling and Simulation in Materials Science and Engineering* 22 (6), 65012.
- Zhao, Z., Bieler, T. R., Llorca, J., Eisenlohr, P., 2020. Grain boundary slip transfer classification and metric selection with artificial neural networks. *Scripta Materialia* 185, 71 – 75.